physica status solidi rrl
www.pss-rapid.com

Robust Electrothermal Switching of Optical Phase-Change Materials through Computer-Aided Adaptive Pulse Optimization

Parth Garud, Kiumars Aryana, Cosmin Constantin Popescu, Steven Vitale, Rashi Sharma, Kathleen A. Richardson, Tian Gu, Juejun Hu, and Hyun Jung Kim**

Electrically tunable optical devices present diverse functionalities for manipulating electromagnetic waves by leveraging elements capable of reversibly switching between different optical states. This adaptability in adjusting their responses to electromagnetic waves after fabrication is crucial for developing more efficient and compact optical systems for a broad range of applications, including sensing, imaging, telecommunications, and data storage. Chalcogenide-based phase-change materials (PCMs) have shown great promise due to their stable, nonvolatile phase transition between amorphous and crystalline states. Nonetheless, optimizing the switching parameters of PCM devices and maintaining their stable operation over thousands of cycles with minimal variation can be challenging. Herein, the critical role of PCM pattern as well as electrical pulse form in achieving reliable and stable switching is reported on, extending the operational lifetime of the device beyond 13000 switching events. To achieve this, a computer-aided algorithm that monitors optical changes in the device and adjusts the applied voltage in accordance with the phase transformation process is developed, thereby significantly enhancing the lifetime of these reconfigurable devices. The findings reveal that patterned PCM structures show significantly higher endurance compared to blanket PCM thin films.

1. Introduction

Achieving postfabrication tunability in micro-optical devices is of broad interest to applications spanning adaptive optics, beam steering, multispectral imaging, heads-up display, and beyond. Such tunability has been implemented with methods such as mechanical stretching,[1] thermo-optic modulation,[2] liquid crystals,[3] and magnetic field biasing[4] in various active materials. Among them, chalcogenide-based phase-change materials (PCMs), a class of active materials exhibiting significantly different optical, electrical, and thermal properties between their crystalline and amorphous states,[5–7] have garnered significant attention due to their nonvolatile phase transformation and large contrast in their refractive index ($\Delta n \approx 1 - 2$).[8] In particular, PCM-based optical metasurfaces have been shown to offer large tunability and allow for pixel level control, a feature not possible with mechanical switching.[9]

Metasurfaces are a class of optical components that have emerged as a driving force in modern optical technology due to their unparalleled capabilities in manipulating light in a more compact configuration. These ultrathin planar structures, composed of subwavelength elements, have redefined conventional optical devices by enabling precise control over light's amplitude, phase, and polarization in a remarkably compact configuration.[10] The compactness and versatility of metasurfaces have propelled them to the forefront of optical engineering, offering solutions to a myriad of challenges

P. Garud, K. Aryana, H. J. Kim
NASA Langley Research Center
Hampton, VA 23681-2199, USA
E-mail: kiumars.aryana@nasa.gov; hyunjung.kim@nasa.gov

P. Garud
Daniel Guggenheim School of Aerospace Engineering
Georgia Institute of Technology
Atlanta, GA 30332, USA

C. C. Popescu, T. Gu, J. Hu
Department of Materials Science and Engineering
Massachusetts Institute of Technology
Cambridge 02139, MA, USA

S. Vitale
Lincoln Laboratory
Massachusetts Institute of Technology
Lexington, MA 02421, USA

R. Sharma, K. A. Richardson
The College of Optics and Photonics
Department of Materials Science and Engineering
University of Central Florida
Orlando, FL 32816, USA

T. Gu, J. Hu
Materials Research Laboratory
Massachusetts Institute of Technology
Cambridge, MA 02139, USA

The ORCID identification number(s) for the author(s) of this article can be found under https://doi.org/10.1002/pssr.202400177.

DOI: 10.1002/pssr.202400177

in various applications. Today, they are poised to revolutionize optical technology, finding applications in reconfigurable logic gates,[11] optical computing,[12] neural networks,[13,14] optical filters,[15–18] beam steering,[19–21] and focusing lenses.[20–24]

Furthermore, the ability to change the properties of the devices without a constant supply of current lowers the power requirements of PCM-based designs. These materials have a rich history, finding early application in optical discs due to their large optical contrast between amorphous and crystalline phases in response to controlled heating stimuli.[25] Several techniques, such as electrical[26–29] or optical pulsing[23,30,31] and thermal annealing,[32,33] have been employed to trigger phase transformation in PCMs.

The integration of PCMs into micro-optical devices such as metasurfaces offers promising avenues in optical manipulation and signal processing,[18,19,34–36] holding great potential for developing compact, lightweight, and nonvolatile tunable devices. This is particularly critical in space explorations, where size, weight, and power considerations are crucial, and highly tunable optical devices could enhance the efficiency of filtering, focusing, and steering light. Despite PCMs being predominantly utilized in small-scale devices like submicron memory cells, their broader application requires scaling these devices to hundreds of microns or larger. However, the process of scaling up PCM-based devices presents challenges in achieving reliable phase switching. This requires high temperatures, exceeding 600 °C for amorphization, as shown in **Figure 1**a, with fast switching timescales on the order of microseconds. As the device size increases, achieving a uniform heating profile across the PCM area becomes an intricate task.[37,38] The pursuit of reliable and rapid phase switching, while mitigating thermal damage to the device, remains a complex challenge.[18,39]

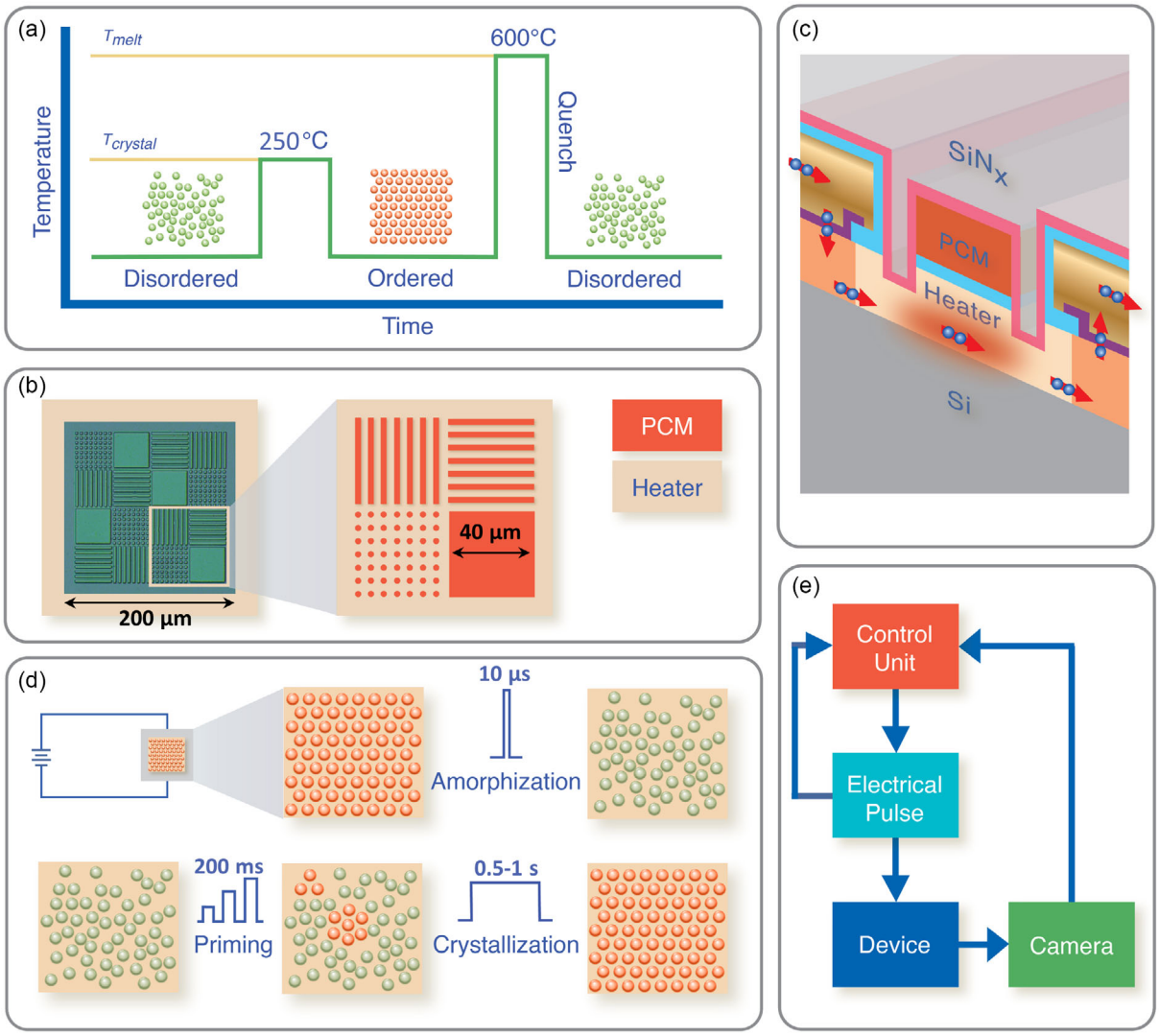

Figure 1. a) Mechanism of phase transformation in PCMs and the necessary temperature rise for each switching event, b) image of the device showing different PCM geometry on a single 200 µm × 200 µm microheater, c) a cross-sectional schematic of the device and the corresponding layers, showing the flow of charges between the electrodes, d) phase transformation mechanism and corresponding pulse shape for crystallization including priming pulse to create nucleation areas[40] and amorphization pulse, and (e) pulse optimization control unit.

In this study, we demonstrate robust switching of PCM-based devices through a computer-aided algorithm that controls the heating pulses with respect to the optical changes in the device, and study the impact of PCM patterns on their switching characteristics. While these devices are not metasurfaces, investigating the behavior of different geometries can provide insight into improving the performance and damage resistance of metasurfaces. For this, three device geometries were investigated: 1) 40 μm × 40 μm blanket-coated thin-film PCM, 2) 40 μm × 3 μm and 40 μm × 2 μm line pattern, and 3) 2 μm circular dot arrays as depicted in Figure 1b. All the geometries are deposited on infrared (IR) transparent microheaters with different sizes 150 μm × 150 μm and 200 μm × 200 μm. This enables us to evaluate the performance of all the configurations under an identical operating condition.

In order to deliver heat and trigger phase transformation, we utilize a doped-Si microheater beneath the PCM that heats up through resistive heating upon application of an electrical pulse. The cross section of the device configuration is shown in Figure 1c. We can control the temperature of the microheater by adjusting the pulse width and amplitude, and thus control the degree of phase transformation in PCM. In this study, we use amorphization pulses that are on the order of 10 μs, while crystallization pulses are lower in amplitude but longer in duration on the order of 0.5–1 s, as shown in Figure 1d. Additionally, we explore the impact of priming pulses—consisting of six consecutive pulses, each 200 ms wide, gradually increasing from 10 V to the crystallization voltage—on the acceleration and uniformity of crystallization within these devices.[40] The performance of the device highly depends on the degree and quality of phase transformation, which is primarily dictated by electrical pulses delivered at the heater. As a result, it is consequential to optimize the pulses in a way that we achieve consistent phase transformation upon each cycle while avoiding damage to the device by overheating. Additionally, PCMs can experience drifts in their properties as they undergo thousands of switching cycles, which causes the optical performance of the PCM-based devices to deviate from their designed states. Thus, it is important to adapt techniques to mitigate this drift in the switching property as the device cycles.

Thus far, there have been limited studies devoted to streamlining the optimization of PCM switching pulse parameters for devices beyond several tens of micrometers, which has largely relied on a trial-and-error process necessitating significant human intervention. These pulses are dependent on the geometry of the microheaters as well as its neighboring materials and thus can vary from one study to another. Manually testing the PCM-based devices to determine the optimal pulses is a time-consuming process, starting from a safe voltage and steadily increasing the amplitude or pulse width to reach maximum switching. In PCM-based devices, it is crucial to apply precisely enough energy to reach the melting temperature to avoid overheating the devices which can lead to premature failure. This process is also prone to human error during manual testing, for example, causing damage upon increasing the voltage by large increments. This can drastically decrease the lifetime of the device.

Although switching cycles in storage-class memory easily exceeds millions of cycles,[41] effectively switching PCM beyond several thousand cycles becomes increasingly challenging as the effective switching size of PCM increases, primarily due to exacerbated temperature nonuniformity across the volume of the PCM. In this article, we strive to achieve consistent and repeatable switching events over thousands of switching cycles by focusing on the PCM pattern geometry as well as pulse optimization through a computer-aided algorithm. This technique not only automates the measurement procedure but also gives feedback to the function generator to adjust the pulses according to the device's behavior. As we will show in this article, the automation process is critical for ensuring the reliable and reproducible operation of these devices. For this, we leverage a feedback loop that monitors the changes in the optical properties of the device using a short-wave IR (SWIR) camera and cautiously adjusts the pulse voltage to maximize optical contrast while mitigating damage. This feedback-driven approach offers a promising solution to the challenges associated with PCM-based micro-optical devices, advancing their capabilities to new heights.

2. Results and Discussion

Our investigation begins with examining a microheater with dimensions of 150 μm × 150 μm that encompasses all three different PCM pattern geometries as depicted in **Figure 2**a. Initially, we try to validate our algorithm implemented in the software by conducting tests on this device, where human operators make decisions on voltage adjustments. The results from this experiment are crucial for optimizing the control logic within the graphical user interface (GUI) and ensuring the computer can replicate human decisions accurately. To prevent damage to the device, we initiate the experiment with a conservative voltage level well below the thresholds for crystallization and amorphization. We begin the crystallization pulses at 15 V and the amorphization pulses at 31 V, gradually raising the pulse voltage until we detect reversible changes in the sample's reflectivity. To evaluate phase transformation, we capture an image from the device before each pulse and take the average reflectivity of the pixels within the region covered by PCM. This average reflectivity of the PCM-covered area as a function of switching event is depicted in Figure 2b, along with the respective applied voltages. The inset provides a closer view of the switching consistency between cycles, after the pulse voltage for crystallization and amorphization reaches sufficient threshold to trigger phase transformation. Note that the voltage is updated only after every 14 switching events. For detailed information on the GUI decision-making logic and the implemented algorithm, please refer to Experimental Section.

At the beginning of the experiment, the amorphization and crystallization pulses were not balanced, i.e., the applied pulses crystallize and amorphize PCM to a different extent, as is apparent in switching events 1–100. Specifically, the crystallization voltage proved insufficient to trigger crystallization of the PCM, while the amorphization voltage gradually increased the amorphized volume. Consequently, this leads to a decrease in reflectance below the initial uncycled state. At this point, the operator increases the crystalline voltage to trigger crystallization. The device then stabilizes in an amorphous state and the

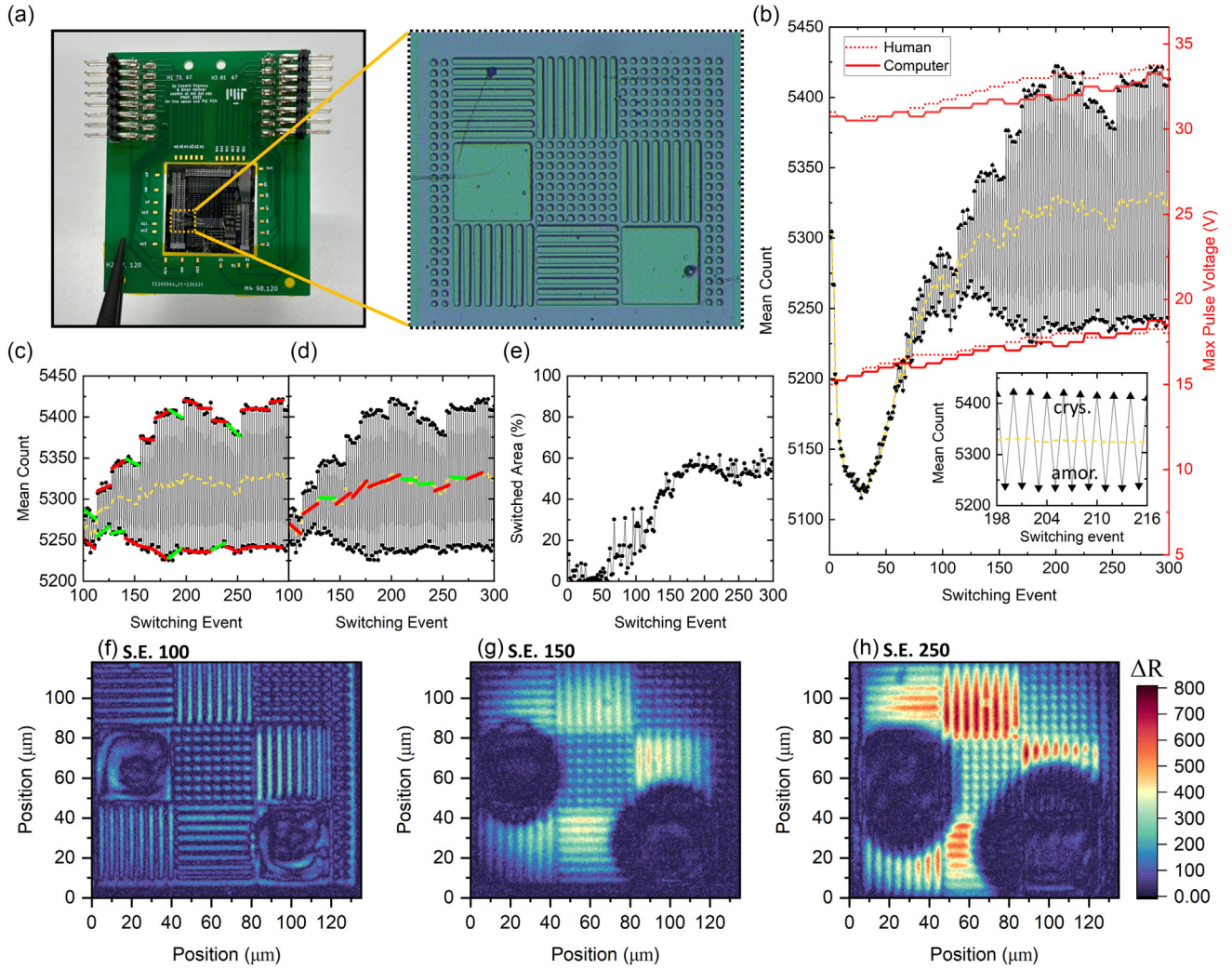

Figure 2. Comparing the pulse optimization process implemented by a human operator and the adaptive algorithm on a PCM device. a) An optical image of a chip containing PCM device arrays mounted on and wire bonded to a custom printed circuit board. The thin film, 1D lines, and 2D dot array PCM patterns on a 150 μm × 150 μm microheater are shown on the right; b) a graph of the mean reflectance values of a PCM device, as well as the pulse voltages applied during the experiment and simulated pulses generated with the software while postprocessing; c) the conditions checked by the software to update the input parameters to ensure equal switching; d) the condition checked by the software to update the input parameters to increase the ΔR; e) the percentage area of the device that is switching; and f–h) the ΔR between the crystalline and amorphous phases at switching events 100, 150, and 250, respectively.

crystallization begins to catch up. Once the device stabilized again around the initial state, the operator continues to observe any trends in either pulse that reduces the reflection contrast (ΔR) and increases the amplitude of that pulse accordingly. Although the experiment was conducted by a human controller, the logic outlined in Section "GUI Development and Pulse Optimization" in Experimental Section was developed with the collected data. The ability of the software to detect these trends in the reflectivity in each phase is shown in Figure 2c. The green lines indicate trends that the logic detected as lowering the ΔR, while the red lines indicate that the trend was not significant enough to warrant a change in the pulse. This shows a good agreement between the decisions the human operator made and the software performance in adjusting the voltage.

After stabilizing the switching around switching event 100, the operator begins the process of increasing the ΔR by increasing the amplitude of both pulses. In order to ensure that the device is switching consistently, this is only done when the mean value of each cycle is constant. Figure 2d shows a similar logic being implemented while postprocessing the data. A linear fit was applied to the mean reflectance values of sets of 28 switching events. This longer duration was chosen to be more cautious and ensure that the device was stable. The green lines indicate regions where this criterion was satisfied and the red lines mark groups that did not meet this consistency check. These evaluations showed good agreement with the decisions the human operator had made during the experiment when trying to increase the ΔR. After running these switching criteria checks

in the results postprocessing for this device and several other similar devices (refer to Note S1, Supporting Information), these conditions proved to be a good representation of the input parameter changes the human operator made. The computer-generated pulses are shown in Figure 2b and can be compared to the human-operated pulses. The computer mimicked the human decisions at each 14th switching event closely and erred on the side of caution when it deviated.

As the device was cycled through, the switched area of the heater grew as well. The percentage area of the device switching as the experiment progressed is shown in Figure 2e. The maximum value reached was around 50%. Once a large ΔR was achieved, the experiment was terminated after 300 switching events. A pixel was assumed to be switching if it had a ΔR of at least 100 counts to avoid capturing noise in the camera as a switched region. This is a reasonable assumption considering the color maps in Figure 2f–h where the areas with adequate contrast show a close representation of the actual PCM patterns. Even with the small number of switching events, the phase transformation behaviors of the three PCM patterns differ considerably. It can be seen from Figure 2f–h that although the change in mean reflectance for the device increases upon cycling, the unpatterned PCM thin film regions on the device begin to delaminate and the corresponding damage spreads to the other areas of the device as the device was cycled further. However, the line and dot array patterns showed much more resilience and were less prone to delamination.

The investigation into the behavior of PCM devices revealed significant differences in switching characteristics among various geometries. Notably, larger PCM regions tend to require higher switching voltages, which can be attributed to their larger thermal mass. This observation underscores the challenge of achieving uniform switching across nonuniform PCM geometries, which is particularly relevant for applications such as beam-focusing metasurfaces where precise control over switching several different PCM pattern geometries is crucial.

Once we verified the logic for controlling the applied pulses is operating as expected, we moved to a different device to implement the adaptive pulse optimization and evaluate the performance of the device for computer-based control. For this, we use a larger microheater 200 μm × 200 μm, as shown in **Figure 3**a. This device consisted of 40 μm × 40 μm square thin film regions, 40 μm × 2 μm 1D lines, and 2 μm × 2 μm 2D dot arrays. The image in Figure 3b was taken after cycling the device for 7000 switching events, and shows the damage on the device due to delamination. Figure 3c is provided as a reference for the IR image of the device prior to cycling. Figure 3d–f demonstrates the formation of delamination areas in a central thin film region, which propagates from the thin films to the surrounding regions. The footprint of the damage increases toward the end of the experiment, respectively.

This device was cycled for 7000 switching events, and the average device reflectivity is over the course of the experiment, as shown in Figure 3g. The ΔR decreased as it was cycled past 500 switching events. This trend was due to the reduction of the switching area, not a drop in the contrast in areas where delamination did not occur and the PCM continued to switch. Figure 3i shows the percentage of the device's area that was switching, and due to the spread of the damage, the value steadily decreases. The ΔR at the healthy part of the device, shown in Figure 3i, maintains about 40% switching for the full duration of the experiment. This indicates that if the delamination damage spread could have been mitigated, it may have been possible to sustain a large ΔR for the full device.

Given that patterned PCM exhibits superior endurance compared to blanket PCM films against delamination damage, we postulate that a device consisting solely of PCM patterns will significantly outperform the previously discussed devices. This is verified by our experimental results using devices that contain exclusively 1D line patterns as illustrated in **Figure 4**a, featuring dimensions of 2 μm × 40 μm for the upper half and 3 μm × 40 μm for the lower half, onto a 200 μm × 200 μm microheater. Figure 4b–d demonstrates the contrast between images taken after crystallization and amorphization by the SWIR camera. Essentially, these images represent the difference in reflectivity of the PCM ($\Delta R = |R_{\text{crys}} - R_{\text{amor}}|$) between the crystalline and amorphous phases at switching events 125, 1250, and 12 500. Brighter areas indicate a more significant change in PCM reflectivity during the switching event, which suggests a stronger phase transformation.

Similar to previous measurements, we begin the experiment with low voltage pulses and gradually raise the voltage to detect changes in the reflectivity. Figure 4e shows the mean reflectivity as a function of switching event for the entire heater area. A video demonstrating the switching process and damage formation is available in the Supporting Information. The corresponding pulse voltages as well as the heater resistance are plotted in Figure 4f. According to our observations, the reflectivity of the PCM-covered area on the microheater remains unchanged during the first few tens of cycles. However, as the pulses reach 17 V for crystallization and 40 V for amorphization, we start to detect minor shifts in the reflectivity of the lines, as shown in Figure 4e. As we increase the voltage further, we observe a larger contrast in reflectivity between the amorphous and crystalline states. However, at switching event 399, we notice that a small portion of the sample stops switching upon phase transformation, and this region expands further during cycling, as depicted in Figure 4c at switching event 1250. As the device continues to be cycled, the algorithm detects slight changes in the reflectance and adjusts the parameters accordingly. These deviations were recognized by the computer after thousands of cycles of consistent switching. Detecting these would be difficult for a human, given their slow and lengthy nature, underscoring the utility of using a computer-aided algorithm to optimize and maintain the switching of the device. Toward the end of the experiment, the resistance decreased slightly but then increased drastically, as shown in Figure 4g. This drastic increase in resistance is due to the damage to the heater.

Figure 4h shows the maximum switching area covered by the PCM as a function of switching event. Initially, the switching area increases gradually and peaks at approximately the 200th switching event, with over 90% of the device area undergoing a phase transformation. Over the following 200 switching events, the switching area remains consistent before signs of damage begin to appear. As the damaged area enlarges, the maximum switching area decreases until the 1000th switching event. Following this, it maintains a relatively steady level until the

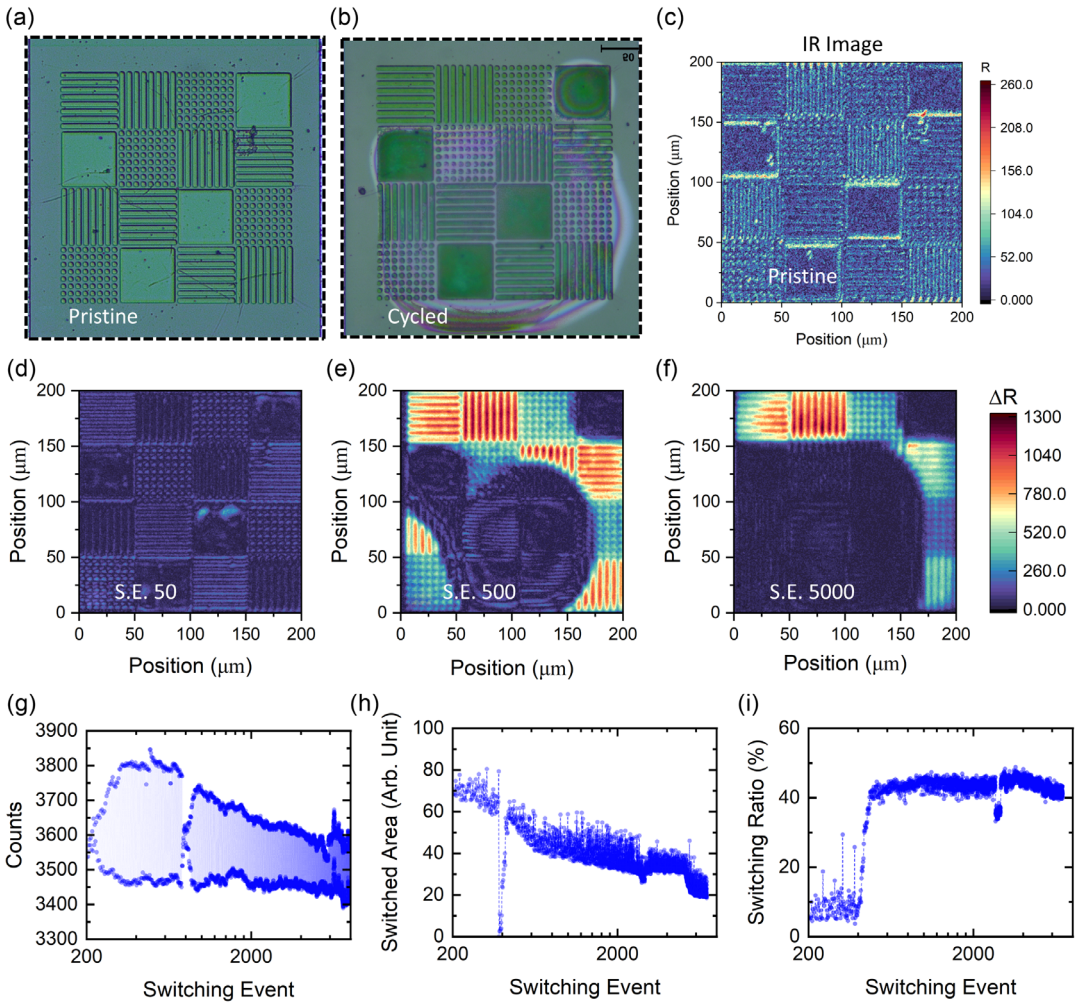

Figure 3. PCM device switching performance using the adaptive pulse optimization algorithm. a) An optical image of a device taken before the experiment featuring PCM thin film, 1D line, and 2D dot array geometries on a 200 μm × 200 μm microheater; b) an optical image of the device taken after the experiment; c) SWIR image of the device in its as-deposited state taken prior to the start of the experiment; d–f) the ΔR between the crystalline and amorphous phases at switching events 50, 500, and 5000 switching events respectively; g) the average reflectance of the device as a function of switching event; h) the area of the device that is switching as a function of switching event; and i) the switching ratio of the pixel with the largest switching value.

device eventually fails. In Figure 4i, the maximum switching ratio (R_c/R_a) is depicted as a function of switching event. Here, we focus on the most substantial contrast, irrespective of the switching area, which could be as small as one pixel. This parameter signifies that in an ideal scenario where we could achieve perfect PCM switching uniformly across the entire microheater area, we would observe nearly a 50% change in reflectance at the operating wavelength of the camera. Figure 4j shows an image of the device at the conclusion of the experiment. The damage in the heater due to electromigration of the metal contact is evident in the blackened regions visible on the right half of the device.

Throughout the cycling experiment, the GUI facilitated dynamic adjustments to input voltages in response to changes in the desired reflectance delta, ensuring optimal device performance. Of particular significance is the observation of PCM exhibiting good switching performance toward the end of the experiment, with a maximum optical contrast nearing 1000 counts. This shows the benefits of managing the input parameters with the GUI to avoid prematurely overstressing the device due to human errors and impatience. This experiment was repeated for another similar pad, and the results of that test have been included in Note S2, Supporting Information.

We can see that the patterned PCM, i.e., the lines and dot arrays, demonstrated greater resistance to damage propagation compared to unpatterned thin films. In previous assessments of PCM devices that were continuous films, damage propagation occurred rapidly following initial delamination.[18,38,42] In contrast, the patterned PCM demonstrated distinct damage mitigation patterns. These findings emphasize the intricate interplay between PCM geometry, switching behavior, and device durability. This improved durability may be attributed to the presence of direct contact areas between the Al_2O_3/SiN capping layer and the heater in patterned PCM regions. As a result of better adhesion between the capping layer and Si heater compared to that between PCM and heater, localized delamination in the

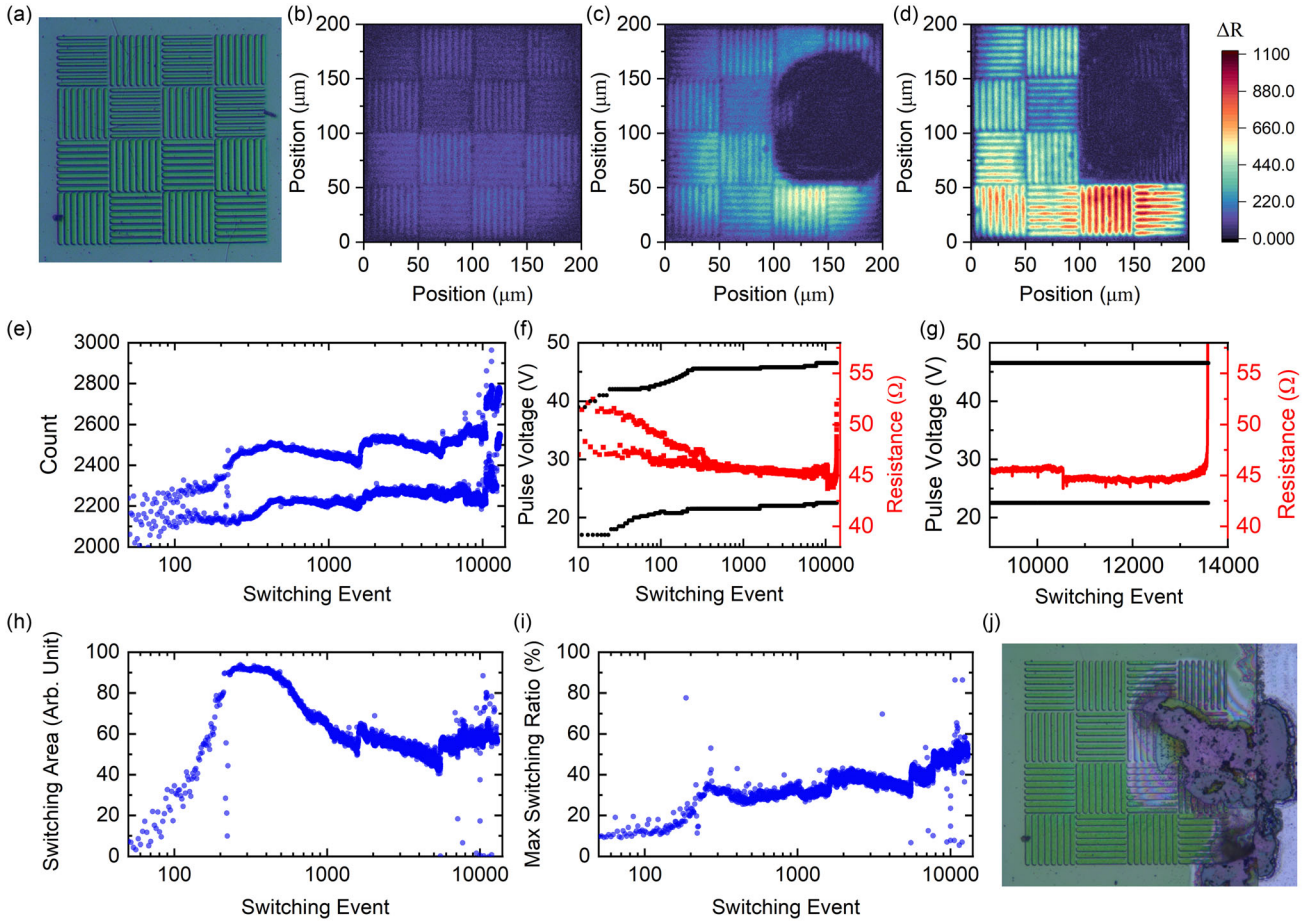

Figure 4. Demonstrating enhanced endurance in a device containing only 1D line pattern PCM geometries. a) An image of a device featuring 2 μm (upper half) and 3 μm (lower half) gratings on a 200 μm × 200 μm microheater; b–d) switching contrast images of the device contrast at switching events 125, 1250, and 12 500, respectively; e) the mean reflectance of the healthy PCM regions of the device as a function of switching event; f) the prescribed voltages and measured resistances during the experiment; g) the prescribed voltages and measured resistances at the end of the experiment; h) the device area switching as a function of switching event; i) the ratio of the reflectivity in crystalline to amorphous phase for the pixel with the maximum switching each switching event; and j) an image of the device taken at the conclusion of the cycling.

patterned areas minimally affects neighboring regions. This highlights the potential of these geometries for applications requiring prolonged device lifetimes and reliable performance.

In conclusion, using a systematic approach, we developed a GUI to automate measurements and control pulse amplitudes, carefully pushing the device to its maximum contrast between phases while minimizing damage. Our results indicate that blanket-coated PCM films are highly prone to delamination due to weak adhesion between the PCM and heater, whereas patterned structures such as lines and dot arrays exhibit greater resilience over repeated cycles. This is attributed to the direct contact between the encapsulating layer and heater in the patterned regions, which enhances robustness and effectively prevents the propagation of damage. Notably, we achieved over 13 000 switching events for PCM line patterns on a 200 μm × 200 μm microheater. This underscores the benefit of using microstructured PCM architectures such as diffraction gratings and metasurfaces for device longevity, as it provides locations where the encapsulating layer can directly bond to the heater underneath, acting as pillars to inhibit damage spread. Our findings will contribute to enhancing the reliability of electrically switchable PCM micro-optical devices toward their practical deployment.

3. Disclaimer

Specific vendor and manufacturer names are explicitly mentioned only to accurately describe the test hardware. The use of vendor and manufacturer names does not imply an endorsement by the U.S. Government nor does it imply that the specified equipment is the best available.

4. Experimental Section

Device Fabrication: The doped silicon heaters were fabricated at the MIT Lincoln Laboratory and details of the fabrication process can be found in our prior works.[43,44] In short, silicon-on-insulator wafers with 1 μm buried

oxide and 155 nm of silicon were doped via ion implantation before metallization with a Ti/TiN liner and 200 nm of Al layer for electrodes. The chip was then prepatterned via photolithography and the phase-change alloy $Ge_2Sb_2Se_4Te$ (GSST)[45,46] was deposited via thermal evaporation and patterned using lift-off. The thermal evaporation was performed at a base pressure below 2×10^{-6} Torr at a maximum deposition rate of ≈ 8 Å s^{-1} The deposition was performed from preweighted source materials prepared using a melt-quench technique and crushed into powders. The target thickness was 180 nm. After the lift-off in *N*-methylpyrrolidone, the GSST patterns were capped at 150° C in 20 nm of atomic layer deposited Al_2O_3 and further encapsulated via reactive sputtering with 800 nm of SiN_x. Fluorine-based reactive ion etching was used to open windows on the contact pads so the aluminum can be accessed again for wire-bonding and testing.

Experimental Setup: In order to monitor the device as it undergoes phase transformation, we used a SWIR camera (FLIR A6262) that operates in the wavelength range of 600–1700 nm. We used a long pass filter at 800 nm to only capture the IR portion of the signal. For magnifying the image of the microheater, we used a Navitar zoom lens with a coaxial illuminating port supported by a 10× Mitutoyo objective focusing lens. For this experiment, we monitored the changes in the reflected light from the PCM. For phase transformation, due to the large size of the device compared to PCM-based memory devices, we needed to apply voltages up to 40–50 V to trigger amorphization. For this, we used a function generator (Agilent 33220A) that was coupled with a DC power supply (Keysight E36232A) through a MOSFET switch that allowed us to deliver voltages up to 60 V. We controlled the applied voltage with a computer-aided algorithm that captured an image from the surface of the device after each switching event and analyzed the degree of the phase transformation. Additionally, several other instruments such as a multimeter and oscilloscope were used to monitor the resistance of the heater as well as the pulse shape. Ultimately, all the components and instruments worked cohesively to cycle the device and monitor its health and performance. Additional information can be found in Note S3, Supporting Information.

GUI Development and Pulse Optimization: The experimental procedure for studying phase transformation behavior in PCM-based devices employs an iterative process coupled with real-time data analysis to regulate pulse amplitude in relation to the extent of phase transformation. In this experiment, prior to sending each pulse, an image of the device is captured and analyzed within the software to determine the pulse amplitude in the following cycles. Starting with user-defined input parameters like pulse widths, amplitudes, and interpulse intervals, the software initiates the cycling process. This involves administering priming and crystallization pulses followed by an amorphization pulse to achieve a full cycle.

The software employs a systematic analysis that relies on detecting changes in the reflectance of the PCM-covered surface on the microheater, indicative of the degree of phase transformation in PCM. Linear regression, represented by coefficients $y = m_1x + m_2$, is used to identify trends linked to changes in reflectivity, followed by sending signals to power supply to adjust subsequent pulse amplitudes accordingly. The software updates the pulse parameters every 14 switching events, or 7 cycles. During each set of 14 switching events, the software evaluates the reflectance trends for both amorphous and crystalline states. It then adjusts the subsequent pulse based on the slope of these trends. The software adjusts the pulses every seven cycles either by only 0.25 V. This number is arbitrarily selected so that it is sufficiently small to stop damage before it propagates further into the device. The software also checks mean reflectance values and flatness of the mean switching value to identify regimes of consistent reversible switching. Once such a state is achieved, the pulse amplitudes are increased until a goal $\Delta R$is achieved. This goal for the reflectance contrast is user-specified reflectance contrast.

One crucial parameter for computer-based identification of phase transformation is the reflectance contrast, denoted as ΔR, which is determined by subtracting the amplitude of the response from each pixel in the camera's image in the amorphous phase from that in the crystalline phase. The user can define a target value for how much switching (in counts) is desired per cycle. This target value generally comes from prior tests and how much change in reflectance could be achieved for a given PCM composition. If this number is too small, we would expect only partial crystallization/amorphization, while if the number is too large, the software will keep raising the voltage beyond the device tolerance and would lead to failure. Additionally, the geometry and performance requirements of the device must be considered when deciding what the target reflectance delta should be. For example, a device consisting of only the 2D dot array pattern would achieve a lower mean switching value than one consisting of only thin films due to the lower areal fill factor of PCM.

The algorithm assesses changes in the reflectivity of the device based on the user specified ΔR to decide whether to adjust voltage levels or maintain them. Another important parameter in the implemented algorithm is the healthy switchable area, which is defined as the area that consistently exhibits reversible changes in reflectance during cycling. The areas that are not showing any change in the reflectivity either have not been heated enough, indicating a need for more voltage to switch, or have been damaged. It is very important that the software detects damage before it propagates further and decrease the voltage accordingly. For this, we monitor the number of pixels that had already exhibited sufficient switching. Ideally, this number must increase in the beginning of the cycling process and stays flat for the reminder of the process before the damage occurs. For more details about the algorithm implementation and Github source, refer to Note S4, Supporting Information.

Supporting Information

Supporting Information is available from the Wiley Online Library or from the author.

Acknowledgements

P.G. and K.A. contributed equally to this work. The authors appreciate the support by Mr. Ronald Neale and Mr. Stanley H. Husch in graphic design and Mr. William Humphreys, chief engineer at NASA LaRC, for review with substantial feedback on the article. P.G. performed his work while an intern funded through the NASA Office of STEM Engagement. K.A. performed his work funded by the NASA Postdoctoral Program (NPP) through Oak Ridge Associated Universities (ORAU). This research was sponsored by the National Aeronautics and Space Administration (NASA) through a contract with ORAU and by the National Science Foundation under Awards 2132929 and 2225968. This work was carried out in part through the use of MIT.nano's facilities. The views and conclusions contained in this document are those of the authors and should not be interpreted as representing the official policies, either expressed or implied, of the NASA or the U.S. Government. The U.S. Government is authorized to reproduce and distribute reprints for government purposes notwithstanding any copyright notation herein.

Conflict of Interest

The authors declare no conflict of interest.

Data Availability Statement

The data that support the findings of this study are available from the corresponding author upon reasonable request.

Keywords

chalcogenide-based phase-change materials, integrated circuits, metasurfaces, microscale devices

Received: May 21, 2024
Revised: May 23, 2024
Published online:

[1] I. M. Pryce, K. Aydin, Y. A. Kelaita, R. M. Briggs, H. A. Atwater, *Nano Lett.* **2010**, *10*, 4222.
[2] S. A. Miller, Y.-C. Chang, C. T. Phare, M. C. Shin, M. Zadka, S. P. Roberts, B. Stern, X. Ji, A. Mohanty, O. A. J. Gordillo, U. D. Dave, M. Lipson, *Optica* **2020**, *7*, 3.
[3] H. K. Bisoyi, Q. Li, *Chem. Rev.* **2021**, *122*, 4887.
[4] J. Valente, J.-Y. Ou, E. Plum, I. J. Youngs, N. I. Zheludev, *Nat. Commun.* **2015**, *6*, 7021.
[5] S. Raoux, *Annu. Rev. Mater. Res.* **2009**, *39*, 25.
[6] M. Wuttig, H. Bhaskaran, T. Taubner, *Nat. Photon.* **2017**, *11*, 465.
[7] K. Aryana, J. T. Gaskins, J. Nag, D. A. Stewart, Z. Bai, S. Mukhopadhyay, J. C. Read, D. H. Olson, E. R. Hoglund, J. M. Howe, A. Giri, M. K. Grobis, P. E. Hopkins, *Nat. Commun.* **2021**, *12*, 774.
[8] K. Aryana, H. J. Kim, M. R. Islam, N. Hong, C.-C. Popescu, S. Makarem, T. Gu, J. Hu, P. E. Hopkins, *Opt. Mater. Express* **2023**, *13*, 3277.
[9] M. Y. Shalaginov, S. D. Campbell, S. An, Y. Zhang, C. Ros, E. B. Whiting, Y. Wu, L. Kang, B. Zheng, C. Fowler, H. Zhang, D. H. Werner, J. Hu, T. Gu, *Nanophotonics* **2020**, *9*, 3505.
[10] N. Yu, F. Capasso, *Nat. Mater.* **2014**, *13*, 139.
[11] Y. Zhang, Z. Peng, Z. Wang, Y. Wu, Y. Hu, J. Wu, J. Yang, *Nanomaterials* **2023**, *13*, 1375.
[12] F. Brückerhoff-Plückelmann, J. Feldmann, C. D. Wright, H. Bhaskaran, W. H. Pernice, *J. Appl. Phys.* **2021**, *129*, 15.
[13] J. Feldmann, N. Youngblood, C. D. Wright, H. Bhaskaran, W. H. Pernice, *Nature* **2019**, *569*, 208.
[14] Y. Shen, N. C. Harris, S. Skirlo, M. Prabhu, T. Baehr-Jones, M. Hochberg, X. Sun, S. Zhao, H. Larochelle, D. Englund, M. Soljacic, *Nat. Photon.* **2017**, *11*, 441.
[15] K. V. Sreekanth, R. Medwal, C. M. Das, M. Gupta, M. Mishra, K.-T. Yong, R. S. Rawat, R. Singh, *Nano Lett.* **2021**, *21*, 4044.
[16] F. Shen, Q. Kang, J. Wang, K. Guo, Q. Zhou, Z. Guo, *Nanomaterials* **2018**, *8*, 938.
[17] M. N. Julian, C. Williams, S. Borg, S. Bartram, H. J. Kim, *Optica* **2020**, *7*, 746.
[18] C. C. Popescu, K. Aryana, P. Garud, K. P. Dao, S. Vitale, V. Liberman, H.-B. Bae, T.-W. Lee, M. Kang, K. A. Richardson, C. A. R. Ocampo, Y. Zhang, T. Gu, J. Hu, H. J. Kim, *Adv. Mater.* **2024**, https://arxiv.org/abs/2312.10468.
[19] P. Moitra, Y. Wang, X. Liang, L. Lu, A. Poh, T. W. Mass, R. E. Simpson, A. I. Kuznetsov, R. Paniagua-Dominguez, *Adv. Mater.* **2023**, *35*, 2205367.
[20] X. Yin, T. Steinle, L. Huang, T. Taubner, M. Wuttig, T. Zentgraf, H. Giessen, *Light: Sci. Appl.* **2017**, *6*, e17016.
[21] T. Roy, S. Zhang, I. W. Jung, M. Troccoli, F. Capasso, D. Lopez, *APL Photon.* **2018**, *3*, 2.
[22] E. Arbabi, A. Arbabi, S. M. Kamali, Y. Horie, M. Faraji-Dana, A. Faraon, *Nat. Commun.* **2018**, *9*, 812.
[23] Q. Wang, E. T. Rogers, B. Gholipour, C.-M. Wang, G. Yuan, J. Teng, N. I. Zheludev, *Nat. Photon.* **2016**, *10*, 60.
[24] W. Zhu, Q. Song, L. Yan, W. Zhang, P.-C. Wu, L. K. Chin, H. Cai, D. P. Tsai, Z. X. Shen, T. W. Deng, S. K. Ting, Y. Gu, G. Q. Lo, D. L. Kwong, Z. C. Yang, R. Huang, A. Liu, N. Zheludevh, *Adv. Mater.* **2015**, *27*, 4739.
[25] M. Wuttig, N. Yamada, *Nat. Mater.* **2007**, *6*, 824.
[26] N. Ciocchini, M. Laudato, M. Boniardi, E. Varesi, P. Fantini, A. L. Lacaita, D. Ielmini, *Sci. Rep.* **2016**, *6*, 29162.
[27] N. Ali, R. Kumar, arXiv:2001.10430, **2020**.
[28] A. Redaelli, A. Pirovano, F. Pellizzer, A. L. Lacaita, D. Ielmini, R. Bez, *IEEE Electron Device Letters* **2004**, *25*, 684.
[29] T. Singh, R. R. Mansour, *IEEE Trans. Microw. Theory Techn.* **2019**, *67*, 3237.
[30] A.-K. U. Michel, P. Zalden, D. N. Chigrin, M. Wuttig, A. M. Lindenberg, T. Taubner, *ACS Photon.* **2014**, *1*, 833.
[31] A. V. Kolobov, P. Fons, A. I. Frenkel, A. L. Ankudinov, J. Tominaga, T. Uruga, *Nat. Mater.* **2004**, *3*, 703.
[32] A. Mandal, Y. Cui, L. McRae, B. Gholipour, *J. Phys. Photon.* **2021**, *2*, 022005.
[33] K. Aryana, Y. Zhang, J. A. Tomko, M. S. B. Hoque, E. R. Hoglund, D. H. Olson, J. Nag, J. C. Read, C. Rios, J. Hu, P. Hopkins, *Nat. Commun.* **2021**, *12*, 7187.
[34] W. Dong, Y. Qiu, X. Zhou, A. Banas, K. Banas, M. B. Breese, T. Cao, R. E. Simpson, *Adv. Opt. Mater.* **2018**, *6*, 1701346.
[35] C. H. Chu, M. L. Tseng, J. Chen, P. C. Wu, Y.-H. Chen, H.-C. Wang, T.-Y. Chen, W. T. Hsieh, H. J. Wu, G. Sun, D. P. Tsai, *Laser Photon. Rev.* **2016**, *10*, 986.
[36] F. Yue, R. Piccoli, M. Y. Shalaginov, T. Gu, K. A. Richardson, R. Morandotti, J. Hu, L. Razzari, *Laser Photon. Rev.* **2021**, *15*, 2000373.
[37] D. Tomer, R. A. Coutu Jr., *Appl. Sci.* **2018**, *8*, 130.
[38] K. Aryana, H. J. Kim, C.-C. Popescu, S. Vitale, H. B. Bae, T. Lee, T. Gu, J. Hu, *Small* **2023**, *19*, 2304145.
[39] Z. Fang, R. Chen, J. E. Fröch, Q. A. Tanguy, A. I. Khan, X. Wu, V. Tara, A. Manna, D. Sharp, C. Munley, F. Miller, Y. Zhao, S. J. Geiger, K. F. Bohringer, M. Reynolds, E. Pop, A. Majumdar, arXiv:2307.12103, **2023**.
[40] J. Orava, A. L. Greer, *Acta Mater.* **2017**, *139*, 226.
[41] C.-C. Popescu, S. Vitale, C. Roberts, P. Miller, K. Aryana, M. Kang, K. Richardson, H. J. Kim, W. Humphreys, T. Gu, J. Hu, in *Photonic and Phononic Properties of Engineered Nanostructures XIII* Vol. *12431*, SPIE, Bellingham, Washington, DC **2023**, pp. 40–48.
[42] K. Ding, J. Wang, Y. Zhou, H. Tian, L. Lu, R. Mazzarello, C. Jia, W. Zhang, F. Rao, E. Ma, *Science* **2019**, *366*, 210.
[43] C.-C. Popescu, K. P. Dao, L. Ranno, B. Mills, L. Martin-Monier, Y. Zhang, D. Bono, B. Neltner, T. Gu, J. Hu, K. Aryana, W. M. Humphreys, H. J. Kim, S. Vitale, P. Miller, C. Roberts, S. Geiger, D. Callahan, M. Moebius, M. Kang, K. A. Rishardson, C. A. R. Ocampo, *Small Sci.* **2023**, *3*, 2300098.
[44] C. Rios, Q. Du, Y. Zhang, C.-C. Popescu, M. Y. Shalaginov, P. Miller, C. Roberts, M. Kang, K. A. Richardson, T. Gu, S. A. Vitale, J. Hu, *PhotoniX* **2022**, *3*, 26.
[45] Y. Zhang, J. Li, J. Chou, Z. Fang, A. Yadav, H. Lin, Q. Du, J. Michon, Z. Han, Y. Huang, H. Zheng, T. Gu, V. Liberman, K. Richardson, J. Hu, in , Optica Publishing Group, Washington, DC **2017**, JTh5C–4.
[46] Y. Zhang, J. B. Chou, J. Li, H. Li, Q. Du, A. Yadav, S. Zhou, M. Y. Shalaginov, Z. Fang, H. Zhong, C. Roberts, P. Robinson, B. Bohlin, C. Rios, H. Lin, M. Kang, T. Gu, J. Warner, V. Liberman, K. Richardson, J. Hu, *Nat. Commun.* **2019**, *10*, 4279.